analytical chemistry

pubs.acs.org/ac

Letter

Exploring Integrin-Mediated Force Transmission during Confined Cell Migration by DNA-Based Tension Probes

Liang Wang, Wei Chen,* Hongyun Li, Chaohui Xiong, Feng Sun, Xiaoqing Liu, Yuru Hu, Wenxu Wang, Wenqun Zhong, and Zheng Liu*

Cite This: *Anal. Chem.* 2022, 94, 4570−4575

Read Online

ACCESS | Metrics & More | Article Recommendations | Supporting Information

ABSTRACT: Mechanical forces have profound effects on the morphology and migration of cells in a two-dimensional environment. However, cells in vivo mostly migrate in three-dimensional space while physically constrained, and the mechanism by which cellular dynamic forces drive migration in this confined environment is unclear. Here, we present a method of fabricating microfluidic chips with integrated DNA-based tension probes to measure spatiotemporal variations in integrin-mediated force exerted during confined cell migration. Using this developed device, we measured the spatial locations, magnitudes, and temporal characteristics of integrin-ligand tension signals in motile cells in different microchannels and found that cells exerted less force and underwent increasingly transitory integrin−ligand interactions when migrating in confined spaces. This study demonstrates that the described method provides insights into understanding the migratory machinery of cells in geometrically confined environment that better mimics physiological conditions.

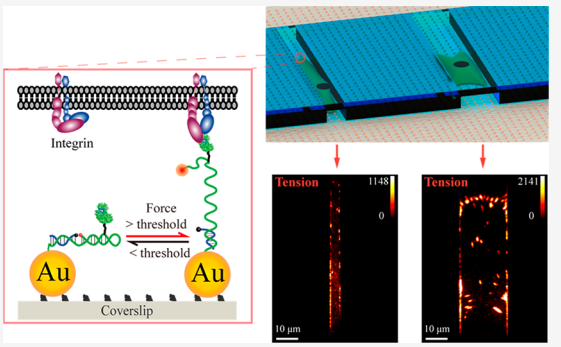

Cell motility affects not only critical biological processes, such as embryonic development[1] and the immune response,[2] but also the progression of various diseases, including cancers.[3] As a direct biophysical interaction between the extracellular matrix (ECM) and cells, mechanical force has been extensively demonstrated to regulate cell migration behaviors,[4] especially on 2D substrates. For instance, force fluctuations mediate directed cell migration along a gradient of ECM stiffness or durotaxis,[5] and integrin-ligand tension is involved in multiple critical steps during mesenchymal cell migration, including the maturation of integrin-mediated adhesion[6] and protrusion of lamellipodia.[7] On the other hand, critical modules in 2D migration, such as focal adhesions (FAs), stress fibers (SFs), and lamellipodia, were found to be reduced or even abolished in cells migrating in a confined space that mimics the in vivo 3D environment,[8−10] and the activity of proteins that regulate motility also seems to differ substantially.[11−13] Thus, these differences in migratory behaviors suggest that further experiments are still needed to expand the knowledge base on the role of force in the migratory machinery under the physical constraints in the physiological environment.

Inspired by the vital role of force in cell motility on 2D substrates, researchers have been attempting to further explore whether physical forces are involved in regulating confinement-induced migratory responses. Raman et al. fabricated a microfluidic chip integrated with micropost-based traction force microscopy (TFM) and found a negative correlation between the width of the microchannels and the average traction, which was diminished by a myosin II inhibitor.[14] Using similar devices, Desvignes et al. discovered that macrophages under confinement conditions exhibited distinct traction characteristics close to the nucleus and in the cellular rim, and the distinctions further varied with the microchannel width.[15] Altogether, while the traction force exhibits a clear correlation with confinement, the proposed TFM-integrated microfluidic chip enabled only force measurement with nN/sub nN force sensitivity and μm spatial resolution due to the diffraction limit and micropost dimensions.[16] Thus, to date, researchers have not yet assessed the molecular integrin−ligand interaction force during confined cell migration, which hinders further exploration of the mechanism in the interplay of confinement and migration at the molecular level.

Recently, molecular tension fluorescence microscopy with pN sensitivity and nm spatial resolution, pioneered by the Salaita laboratory,[17] has been widely used for probing the mechanical forces transmitted on individual membrane proteins in living cells and is transforming the study of mechanobiology.[18] In the past few years, different types of reversible molecular tension probes fabricated with polyethylene glycol (PEG),[19] nucleic acids,[20,21] or engineered peptides[22] as molecular springs have

Received: November 15, 2021
Accepted: March 1, 2022
Published: March 8, 2022

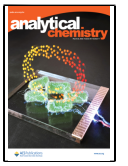

https://doi.org/10.1021/acs.analchem.1c04962
Anal. Chem. 2022, 94, 4570−4575

been applied in different settings. In particular, DNA hairpin-based tension probes,[23,24] benefiting from high sensitivity and digital response advantages, have been widely used to reveal mechanobiology functions in integrin-mediated cell adhesion at the molecular level,[25,26] T cell receptor activation,[27,28] etc. More recently, to address the limited range of conventional DNA hairpin probes (<20 pN), our group reported a reversible shearing DNA-based tension probe (RSDTP) for probing molecular forces between 4 and 60 pN in living cells, thus enabling us to easily distinguish the force-bearing integrins in FAs without perturbing adhesion biology.[29] In this paper, we report a method to fabricate microfluidic chips with newly developed RSDTPs integrated for visualizing integrin-mediated forces during confined cell migration. This combination device overcomes limitations on the sensitivity and spatial resolution of existing force measurements during confined cell migration and enables the visualization of cellular adhesion forces carried by a single integrin in microchannels. By comparing the spatiotemporal information reported by DNA tension probes, we found that confinement not only suppresses the amount of loaded integrins but also alters their tension distribution, spatial distribution, and dynamic features, thus demonstrating the correlation between the force and confined migratory behavior.

EXPERIMENTAL SECTION

Device Fabrication. To produce high-quality integrin tension maps of cells migrating in confined spaces, we developed a fabrication process for reliably and efficiently introducing DNA tension probes into a conventional microfluidic chip as illustrated in Figure 1a. First, a coverslip immobilized with gold nanoparticles (Au NPs) of 5 nm in diameter was prepared following previously described methods.[19,27] A Si-SU8 mold and related PDMS replica were then designed and fabricated based on the approach presented by the Konstantopoulos laboratory.[30] Next, to ensure the integrity of the coated Au NPs on the coverslip, only the PDMS replica was briefly treated with oxygen plasma for 30 s and then bonded firmly to the coverslip, thus forming microchannels with predefined dimensions and Au NP-functionalized substrates. Notably, in contrast to the introduction of Au NPs after PDMS replica-coverslip bonding, the presented protocol prevented unevenly coated Au NPs resulting from the limited size of the microchannels and did not impair the bonding strength between the PDMS replica and substrate, and the imaging quality of the tension signals, therefore, was substantially improved. Finally, DNA tension probes were attached to the Au NPs on the coverslip by incubating the solution of the probes with the device (Supporting Information, Figure S1).

Migration Experiments. The fabricated PDMS microfluid chips were washed with PBS prior to the addition of 20 μL of cell suspension. After 10 min of incubation to allow cell adhesion, the cell suspension was removed and 20 μL of serum free media was injected into the five flow ports of the chip except for the chemokine port, which was later supplied with complete medium to generate a chemogradient along the microchannel. Thus, seeded cells at the inlet of the constructed device could migrate through the microchannels along the imposed chemokine gradient. The molecular tension carried by integrins during confined migration was reported by the DNA probes with pN sensitivity and optical resolution in real time, as shown in Figure 1b and collected using a Nikon Eclipse Ti2 inverted microscope equipped with a 100× oil objective, an EMCCD camera, and a stage-top live cell incubator.

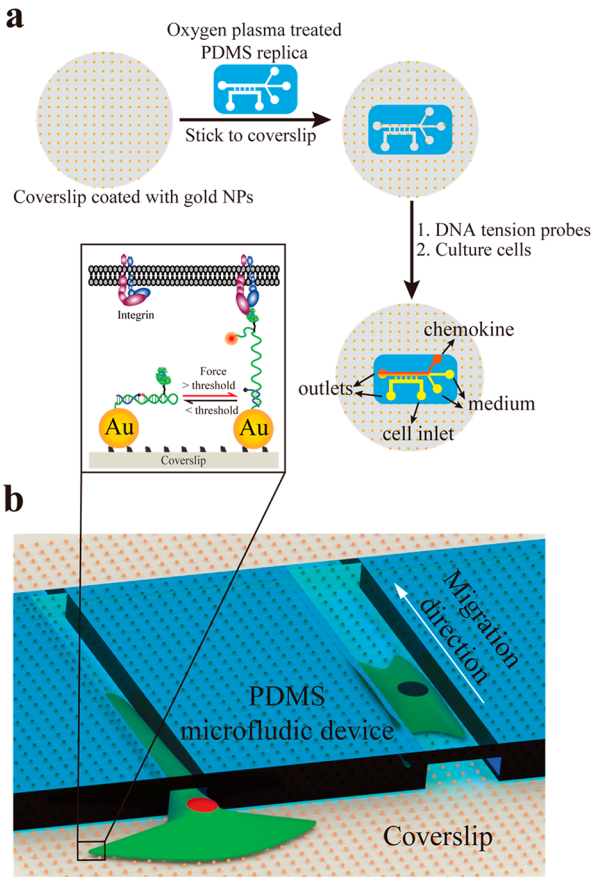

Figure 1. Fabrication of microfluidic devices with DNA tension probes integrated. Schematic depicting (a) procedures to prepare the devices and (b) measurement of integrin tensions using DNA tension probes.

RESULTS AND DISCUSSION

To test the functionality of the device, we imaged the interface between the PDMS chip and the coverslip using reflection interference contrast microscopy (RICM) and 17 pN RSDTPs signals emitted by A375 cells (human malignant melanoma cell line) entering and existing in a microchannel of 200 μm × 5 μm × 10 μm (length × width × height) using total internal reflection fluorescence (TIRF), as shown in Figure S2. The clear boundary of the microchannel in the RICM image demonstrates that the coated Au NPs did not affect the sealing or confinement and thus formed a stable chemokine gradient (Figure S2). TIRF images of the tension signals confirm that this device provided detailed information on integrin tension at high resolution and signal-to-noise ratios. Interestingly, the outside and inside portions of the A375 cells maintain distinct tension phenotypes. Integrin tension signals form large and round clusters, or plaques, spreading along the rim of the outside portion of the cell (magnified images of boxed regions 1 and 4 in Figure S2d,e), while inside the microchannels, they are sparsely located on microchannel boundaries, forming bright strips along the edge (magnified images of boxed regions 2 and 3 in Figure S2d,e). Similar phenomena were observed with HeLa cells (human cervical carcinoma cell line) and WM793 cells (human melanoma cell line), as shown in Figure S3. Taken together, the presented method allows us to visualize the integrin-transmitted molecular forces during confined migration with piconewton resolution and optical resolution in real time, which

https://doi.org/10.1021/acs.analchem.1c04962
Anal. Chem. 2022, 94, 4570−4575

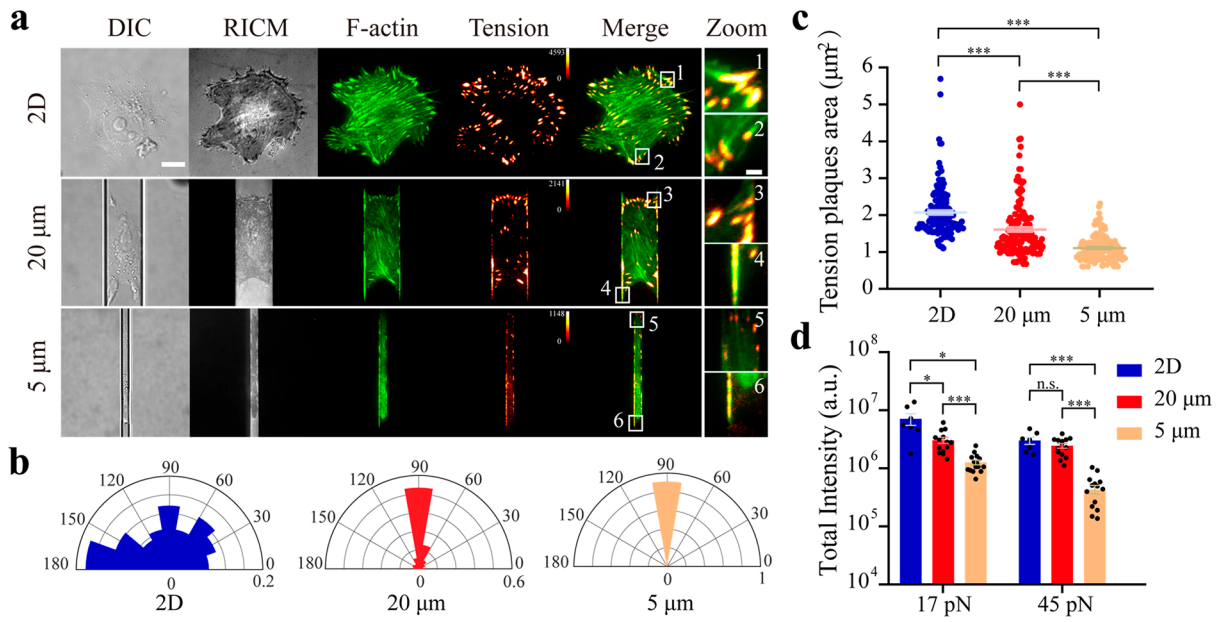

Figure 2. Effects of confinement on cell−ECM interactions. (a) Representative RICM and TIRF images of A375 cells expressing GFP-actin on the planar surface or in microchannels coated with 17 pN DNA probes. Scale bar is 10 μm (2 μm in Zoom). (b) Orientation and (c) area of integrin tension plaques reported by 17 pN RSDTPs under different geometrical confinements are compared using rose plots and scatter plots, respectively (For each confinement level, the number of tension plaques analyzed, $n \geq 140$, from more than 10 cells). (d) Magnitude distribution of integrin tension of cells are quantified using 17 pN and 45 pN. (For each confinement level, number of cells analyzed per probe threshold, $n \geq 7$). Data are mean ± SEM from three independent experiments. Analysis of variance (ANOVA) tests are used to assess statistical significance (***$p < 0.001$, **$p < 0.01$, *$p < 0.05$, not significant (n.s.) $p > 0.05$).

could be critical for understanding the confinement-induced migratory response.

After establishing a method to image the integrin tension of cells in microchannels, we attempted to evaluate the effects of confinement on cell mechanics. To this end, we first examined the morphology, F-actin, and integrin tension in A375 cells transfected with GFP-actin on a nonconfined substrate and in microchannels with widths of 5 or 20 μm. After seeding, cells were induced to migrate along the chemogradient for 4 h to allow the entire cell body to enter the microchannel or incubated on 2D substrates for the same duration before imaging. The morphology, cytoskeleton, and 17 pN tension images of the cells spreading in a nonconfined substrate and microchannels of different widths are presented in Figure 2a.

In both confined settings, cells elongated along microchannels and this pattern was clearly different from the spreading pattern on the 2D substrate. Multiple SFs were formed by the cells on 2D substrates, but actins tended to be diffuse in microchannels. Correspondingly, the spatial distribution of cellular tension in the confined spaces was also significantly different from that of the nonconfined cells. On a 2D substrate, the molecular tension signals of a cell were mainly located evenly around the cell (magnified images of boxed regions 1 and 2 in Figure 2a). In contrast, the distribution of molecular tension signals of the cell was highly related to the microchannel width. In wide microchannels, in addition to the typically large tension signal plaques present in the heads and tails of the cell (magnified images of boxed region 3 in Figure 2a), we found a bright and narrow strip of integrin tension signals distributed along the edges of the microchannels (magnified images of boxed region 4 in Figure 2a). Interestingly, when the microchannel size was further reduced to 5 μm, nearly all the large integrin-mediated tension signals were eliminated (magnified images of boxed region 5 in Figure 2a), and cells only generated weak discontinuous punctate signals on both microchannel edges (magnified images of boxed region 6 in Figure 2a), even though DNA tension probes were homogeneously coated across the microchannels (Supporting Information, Figure S4). Both the orientation, quantified as the angle between the short axis of the ellipse fitted to the plaque and the migration direction, and area of the tension signal pattern confirmed the observation that narrower microchannels tend to induce smaller tension plaques that are more closely aligned with microchannel edges, as shown in Figure 2b,c, respectively. To determine whether myosin contractility dominates these tension signals in a confined microenvironment, we further treated cells in microchannels with the ROCK inhibitor Y27632 (15 nM). The results showed that these diffuse punctate mechanical signals disappeared (Figure S5). Given that Y-27632 can effectively reduce myosin-driven forces, which is similar to the effect of Blebbistatin,[30] our data suggested that tension signal observed in the current confined settings is still a myosin driven force.

To further investigate how the magnitudes of integrin-mediated forces in living cells vary with microchannel size, we repeated the above experiments using both 45 pN and 56 pN RSDTPs (Figure S6a). The results showed that while 56 pN were quite weak and close to the background in all conditions, 45 pN signals seem to change differently compared to 17 pN signals. To further quantify the distinguished sensitivity of 17 pN and 45 pN tension signals to confinement levels, their total fluorescence intensities were analyzed (Supporting Information, Figure S6b), and the results are shown in Figure 2d. A statistical analysis between confinement levels confirmed that although total intensity of 17 pN signals per cell significantly decreases as confinement level increases, 45 pN signals do not drop substantially until in the 5 μm microchannels. These results suggest that integrins carrying different tensions manifest distinct sensitivities to confinement levels, leading to altered

https://doi.org/10.1021/acs.analchem.1c04962
Anal. Chem. 2022, 94, 4570−4575

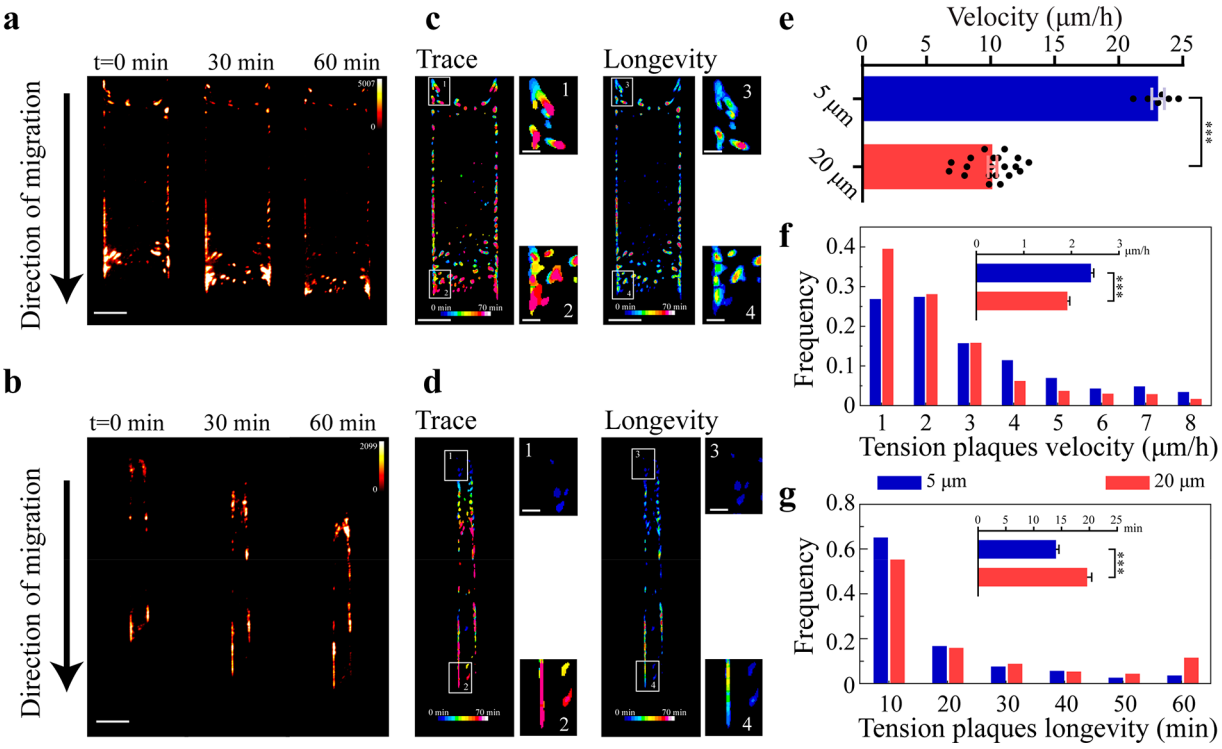

Figure 3. Integrin tensions when cells migrate under different confinements were quantified using time-lapse TIRF microscopy. Representative sequential integrin tensions of A375 cells migrating in microchannels with width of (a) 20 μm and (b) 5 μm are reported by 17 pN RSDTPs. Scale bar is 10 μm (2 μm in Zoom). Traces (left) and lifetime (right) of tension plaques of cells in parts a and b are shown in parts c and d, respectively, to illustrate the dynamic characteristic of individual tension plaques. (e) Migratory velocities of A375 cells (number of cells analyzed, $n \geq 6$), (f) velocity and (g) lifetime distributions of integrin tension plaques in narrow and wide microchannels are compared (for each confinement level, number of tension plaques analyzed, $n \geq 549$, from more than 3 time-lapse videos of 1 h duration at 5 min intervals). Data are mean ± SEM from three independent experiments. Two-tailed Student's t tests are used to assess statistical significance (***$p < 0.001$).

magnitude distribution of the integrin tension signals in a confined environment. For instance, the ratio of the mean total intensity of 45 pN signals per cell to 17 pN signals per cell decreases from 0.80 in the 20 μm microchannel to 0.34 in the 5 μm microchannel. Similar confinement-induced suppression of integrin tension was also observed in WM793 cells (Figure S7). Altogether, these results demonstrate that confinement suppresses integrin forces in cells and alters the tension distributions and spatial characteristics of cell mechanics.

Next, to explore the dynamic behavior of integrin-mediated forces in confined spaces, we performed time-lapse recordings to monitor changes in the 17 pN tension maps of cells in microchannels with widths of 20 and 5 μm (Supplementary Video). First, we observed that the cell migration process in the wide microchannel involved consecutive head protrusions and tail retractions, which are typical of mesenchymal cell migration[31] (Figure 3a). Interestingly, in the narrow microchannel, cells moved not only faster (Figure 3e) but also more smoothly, as the length of the cell did not change significantly during migration with well-coordinated motion of its head and tail (Figure 3b). These distinct migratory behaviors in varied confined settings were also present in WM793 cells (Figure S8). In addition, discrepancies were more apparent by examining traces (Figure 3c,d, left) and longevity (Figure 3c,d, right) of the tension signals during migration. The 17 pN tension signals in wide microchannels tended to move slowly within a small region and remain for a long period (magnified images 3 and 4 in Figure 3c). In contrast, the punctate-like tension signals in the 5 μm microchannels seemed to slide quicker (magnified images 1 and 2 in Figure 3d) with shorter lifetime (magnified images 3 and 4 in Figure 3d). These observations were confirmed by the statistics calculated for tension plaque velocity (Figure 3f) and lifetime (Figure 3g). Cells in wide microchannels clearly maintained a greater percentage of slowly moving but long-lived tension plaques than those in narrow microchannels, indicating that integrin-ligand binding was more dynamic at higher migration velocities. Taken together, these results suggest that confinement drives reductions in integrin forces but increases in the dynamics of integrin−ligand interactions, likely promoting the rate of cell migration.

CONCLUSION

In summary, we developed a fabrication method to integrate DNA-based molecular tension probes into microfluidic chips, in which cells mimic in vivo migratory behaviors much better than those moving on 2D substrates.[32] With these devices, we successfully visualized the integrin tension of cells in microchannels at molecular piconewton resolution for the first time. Compared to existing TFM-based approaches, this method significantly improved the spatial resolution and force sensitivity of force measurement in confined spaces by more than one order of magnitude. We believe the presented method can greatly promote the application of DNA-based tension probes for mechanobiology study under more physiological conditions, such as a geometrically confined environment.

https://doi.org/10.1021/acs.analchem.1c04962
Anal. Chem. 2022, 94, 4570−4575

■ ASSOCIATED CONTENT

Supporting Information

The Supporting Information is available free of charge at https://pubs.acs.org/doi/10.1021/acs.analchem.1c04962.

Methods; Figure S1, structures of RSDTPs and always on probe; Figure S2, characterization and demonstration of fabricated devices; Figure S3, measurements of integrin tensions of multiple cell lines entering microchannels; Figure S4, characterization of immobilized probe density using always on probes; Figure S5, effects of Y27632 on integrin tensions of cells in confinement; Figure S6, representative tension images of A375 cells and data processing flow; Figure S7, confinement-induced changes in integrin tensions of WM793 cells; Figure S8, temporal characteristics of integrin tensions of WM793 cells; and Figure S9, effects of PLL-*g*-PEGs on inhibiting cell adhesion (PDF)

Supplementary Video, representative time-lapse TIRF imaging of 17 pN tension signals performed for A375 cells migrating in microchannels with different widths (AVI)

■ AUTHOR INFORMATION

Corresponding Authors

Zheng Liu − *The Institute for Advanced Studies, Wuhan University, Wuhan 430072, China;* orcid.org/0000-0002-4252-4617; Email: zheng.liu@whu.edu.cn

Wei Chen − *The Institute for Advanced Studies, Wuhan University, Wuhan 430072, China*; Email: w.chen@whu.edu.cn

Authors

Liang Wang − *The Institute for Advanced Studies, Wuhan University, Wuhan 430072, China*

Hongyun Li − *The Institute for Advanced Studies, Wuhan University, Wuhan 430072, China*

Chaohui Xiong − *The Institute for Advanced Studies, Wuhan University, Wuhan 430072, China*

Feng Sun − *The Institute for Advanced Studies, Wuhan University, Wuhan 430072, China*

Xiaoqing Liu − *College of Chemistry and Molecular Sciences, Wuhan University, Wuhan 430072, China;* orcid.org/0000-0002-1309-5454

Yuru Hu − *The Institute for Advanced Studies, Wuhan University, Wuhan 430072, China*

Wenxu Wang − *The Institute for Advanced Studies, Wuhan University, Wuhan 430072, China*

Wenqun Zhong − *Hospital of Stomatology, Wuhan University, Wuhan 430072, China*

Complete contact information is available at: https://pubs.acs.org/10.1021/acs.analchem.1c04962

Notes

The authors declare no competing financial interest.

■ ACKNOWLEDGMENTS

This work was supported by the National Natural Science Foundation of China (Grants 21775115, 32071305, and 32150016), the start-up funding from Wuhan University for financial support, the Fundamental Research Funds for the Central Universities (Grants 2042018kf02, 2042021kf0030, and 2042018kf1006), and Innovation Funds for Postdocs in Hubei Province.

■ REFERENCES

(1) Gilmour, D.; Rembold, M.; Leptin, M. *Nature* **2017**, *541* (7637), 311−320.

(2) Masopust, D.; Schenkel, J. M. *Nat. Rev. Immunol.* **2013**, *13* (5), 309−20.

(3) Wirtz, D.; Konstantopoulos, K.; Searson, P. C. *Nat. Rev. Cancer* **2011**, *11* (7), 512−22.

(4) Charras, G.; Sahai, E. *Nat. Rev. Mol. Cell Biol.* **2014**, *15* (12), 813−24.

(5) Plotnikov, S. V.; Pasapera, A. M.; Sabass, B.; Waterman, C. M. *Cell* **2012**, *151* (7), 1513−27.

(6) Galbraith, C. G.; Yamada, K. M.; Sheetz, M. P. *J. Cell Biol.* **2002**, *159* (4), 695−705.

(7) Bangasser, B. L.; Shamsan, G. A.; Chan, C. E.; Opoku, K. N.; Tuzel, E.; Schlichtmann, B. W.; Kasim, J. A.; Fuller, B. J.; McCullough, B. R.; Rosenfeld, S. S.; Odde, D. J. *Nat. Commun.* **2017**, *8*, 15313.

(8) Balzer, E. M.; Tong, Z.; Paul, C. D.; Hung, W. C.; Stroka, K. M.; Boggs, A. E.; Martin, S. S.; Konstantopoulos, K. *FASEB J.* **2012**, *26* (10), 4045−56.

(9) Holle, A. W.; Govindan Kutty Devi, N.; Clar, K.; Fan, A.; Saif, T.; Kemkemer, R.; Spatz, J. P. *Nano Lett.* **2019**, *19* (4), 2280−2290.

(10) Stroka, K. M.; Jiang, H.; Chen, S. H.; Tong, Z.; Wirtz, D.; Sun, S. X.; Konstantopoulos, K. *Cell* **2014**, *157* (3), 611−23.

(11) Fraley, S. I.; Feng, Y.; Krishnamurthy, R.; Kim, D. H.; Celedon, A.; Longmore, G. D.; Wirtz, D. *Nat. Cell Biol.* **2010**, *12* (6), 598−604.

(12) Doyle, A. D.; Carvajal, N.; Jin, A.; Matsumoto, K.; Yamada, K. M. *Nat. Commun.* **2015**, *6*, 8720.

(13) Hung, W. C.; Yang, J. R.; Yankaskas, C. L.; Wong, B. S.; Wu, P. H.; Pardo-Pastor, C.; Serra, S. A.; Chiang, M. J.; Gu, Z.; Wirtz, D.; Valverde, M. A.; Yang, J. T.; Zhang, J.; Konstantopoulos, K. *Cell Rep.* **2016**, *15* (7), 1430−1441.

(14) Raman, P. S.; Paul, C. D.; Stroka, K. M.; Konstantopoulos, K. *Lab Chip* **2013**, *13* (23), 4599−607.

(15) Desvignes, E.; Bouissou, A.; Laborde, A.; Mangeat, T.; Proag, A.; Vieu, C.; Thibault, C.; Maridonneau-Parini, I.; Poincloux, R. *Nano Lett.* **2018**, *18* (10), 6326−6333.

(16) Roca-Cusachs, P.; Conte, V.; Trepat, X. *Nat. Cell Biol.* **2017**, *19* (7), 742−751.

(17) Stabley, D. R.; Jurchenko, C.; Marshall, S. S.; Salaita, K. S. *Nat. Methods* **2012**, *9* (1), 64−7.

(18) Liu, Y.; Galior, K.; Ma, V. P. Y.; Salaita, K. *Acc. Chem. Res.* **2017**, *50* (12), 2915−2924.

(19) Liu, Y.; Yehl, K.; Narui, Y.; Salaita, K. *J. Am. Chem. Soc.* **2013**, *135* (14), 5320−3.

(20) Zhang, Y.; Ge, C.; Zhu, C.; Salaita, K. *Nat. Commun.* **2014**, *5*, 5167.

(21) Blakely, B. L.; Dumelin, C. E.; Trappmann, B.; McGregor, L. M.; Choi, C. K.; Anthony, P. C.; Duesterberg, V. K.; Baker, B. M.; Block, S. M.; Liu, D. R.; Chen, C. S. *Nat. Methods* **2014**, *11* (12), 1229−32.

(22) Morimatsu, M.; Mekhdjian, A. H.; Adhikari, A. S.; Dunn, A. R. *Nano Lett.* **2013**, *13* (9), 3985−3989.

(23) Ma, V. P.-Y.; Salaita, K. *Small* **2019**, *15* (026), 1900961.

(24) Blanchard, A. T.; Salaita, K. *Science* **2019**, *365* (6458), 1080−1081.

(25) Zhang, Y.; Qiu, Y. Z.; Blanchard, A. T.; Chang, Y.; Brockman, J. M.; Ma, V. P. Y.; Lam, W. A.; Salaita, K. *Proc. Natl. Acad. Sci. U. S. A.* **2018**, *115* (2), 325−330.

(26) Glazier, R.; Brockman, J. M.; Bartle, E.; Mattheyses, A. L.; Destaing, O.; Salaita, K. *Nat. Commun.* **2019**, *10* (1), 4507.

(27) Liu, Y.; Blanchfield, L.; Ma, V. P.; Andargachew, R.; Galior, K.; Liu, Z.; Evavold, B.; Salaita, K. *Proc. Natl. Acad. Sci. U. S. A.* **2016**, *113* (20), 5610−5.

(28) Ma, R.; Kellner, A. V.; Ma, V. P.-Y.; Su, H.; Deal, B. R.; Brockman, J. M.; Salaita, K. *Proc. Natl. Acad. Sci. U. S. A.* **2019**, *116* (34), 16949.

(29) Li, H.; Zhang, C.; Hu, Y.; Liu, P.; Sun, F.; Chen, W.; Zhang, X.; Ma, J.; Wang, W.; Wang, L.; Wu, P.; Liu, Z. *Nat. Cell Biol.* **2021**, *23* (6), 642−651.

(30) Tong, Z.; Balzer, E. M.; Dallas, M. R.; Hung, W. C.; Stebe, K. J.; Konstantopoulos, K. *PLoS One* **2012**, *7* (1), No. e29211.

(31) Ridley, A. J.; Schwartz, M. A.; Burridge, K.; Firtel, R. A.; Ginsberg, M. H.; Borisy, G.; Parsons, J. T.; Horwitz, A. R. *Science* **2003**, *302* (5651), 1704−9.
(32) Yamada, K. M.; Sixt, M. *Nat. Rev. Mol. Cell Biol.* **2019**, *20* (12), 738−752.

https://doi.org/10.1021/acs.analchem.1c04962
Anal. Chem. 2022, 94, 4570−4575